



Hemodynamic and fluid flow analysis of a cerebral aneurysm: a CFD simulation

Ahmed G. Rahma¹ · Talaat Abdelhamid¹

Received: 30 June 2022 / Accepted: 3 January 2023

Published online: 24 January 2023

© This is a U.S. Government work and not under copyright protection in the US; foreign copyright protection may apply 2023 **OPEN**

Abstract

In this study, we investigate the hemodynamics parameters and their impact on the aneurysm rupture. The simulations are performed on an ideal (benchmark) and realistic model for the intracranial aneurysm that appears at the anterior communicating artery. The realistic geometry was reconstructed from patient-specific cerebral arteries. The computational fluid dynamics simulations are utilized to investigate the hemodynamic parameters such as flow recirculation, wall shear stress, and wall pressure. The boundary conditions are measured from the patient using ultrasonography. The solution of the governing equations is obtained by using the ANSYS-FLUENT 19.2 package. The CFD results indicate that the flow recirculation appears in the aneurysms zone. The effect of the flow recirculation on the bulge hemodynamics wall parameters is discussed to identify the rupture zone.

Highlights

- The presence of the aneurysms in the patient's vascular system leads presence of a flow vortex inside the bulge. The flow recirculation occurs due to separation at the rear edge of the aneurysm.
- The flow-wall interaction due to the flow recirculation produce uneven variation in the wall shear stress (WSS), which help to investigate the region of the rupture.
- The wall pressure and the wall shear stress have a qualitative similarity in their behavior.

Keywords Hemodynamics · Intracranial aneurysms · Computational fluid dynamics · Flow recirculation · Wall shear stress

1 Introduction

Hemodynamic analysis of the vascular systems of the patients introduced a significant value to understand and diagnose its diseases [1, 2] such as stenosis [3], aneurysms [4] (such as fusiform [5], saccular, false and dissection types [6]), and atherosclerosis. The computational fluid dynamics (CFD) simulations for the hemodynamic analysis are used to investigate various parameters such as the flow structure, recirculation flow, wall pressure, and wall shear

stress (WSS) [7–9]. These simulations are done using two different branches complementing each other. These two branches are based on the used computational domain (Model) [10, 11], the benchmarks (simplifies models) [12–14] and the realistic models (based on a patient-specific vascular system) [15–17]. Cebral et al. evaluated the realistic flow passes reconstructed from Digital Subtraction Angiography (DSA) to present the blood flow structure in an intracranial aneurysm (saccular aneurysm type). The DSA obtained from 15 patient's cerebral arteries with

✉ Talaat Abdelhamid, Talaat_abdelhamid@el-eng.menofia.edu.eg | ¹Physics and Mathematical Engineering Department, Faculty of Electronic Engineering, Menoufiya University, Menouf 32952, Egypt.



15 cerebral aneurysms. Their obtained results show a similarity with the DSA and the CFD reaches 78% [18]. Xiang et al. investigated the hemodynamics role in the rupture of the intracranial aneurysms. The results show that the CFD simulation models are accurate to predict the intracranial aneurysm risk assessment in case of availability of actual database [19]. Bauer et al. investigated the WSS of an aneurysm (Fusiform aneurysms type) using two different flow regimes. The flow regimens implemented the pulsatile flow regime and the transitional regime. Besides the CFD, the experimental work was done using magnetic resonance velocimetry (MRV) and laser Doppler velocimetry (LDV). The results of the CFD and the LDV show an excellent similarity. The WSS temporal and spatial distribution is highly affected by the vortex formation, where the maximum value of the WSS is located at the zone where the vortex is initialized. A laminar flow is shown at the undilated zone and transitional zone (laminar-turbulent) at the aneurysm [20].

Investigation the effect of the blood flow parameters such as the flow recirculation, wall pressure, and WSS on the hemodynamics of the vascular diseases is an important issue [21]. Iimuro et al. conducted a numerical simulation for the portal venous system aneurysms that appears in 75-years woman patient. The simulations were performed using ANSYS FLUENT package software. The simulations are conducted at blood flow rate 1000 mL/min. The results show presence of recirculation flow (turbulences) inside the aneurysms, and the WSS increased at the wall of the aneurysms. The presence of these parameters could lead to creating thrombosis or rupture of the aneurysms [22].

The intracranial aneurysms (IA) are dilations (bulge) in the intracranial arteries vessel due to the blood vessel wall weakness. These cases appears in range of 0.5–6% for the population worldwide [23–25]. The rupture of the intracranial aneurysms (IA) happen for approximately 0.25% of these IAs. About 60% of these rupture cases could face death [26, 27]. Shishir et al. investigated the blood flow dynamics in a human arterial with a saccular aneurysm at the bend. The CFD simulations were done for simplified models with different aneurysm diameters varying from 5 to 8 mm. The simulations are conducted at $Re = 110$ – 850 , specific mass = 1008 kg.m^{-3} , blood flow rate 3.6 mL/s, velocity value = 0.2365 m/s , and viscosity of $0.0035 \text{ N/m}^2\text{s}^2$. The problem implemented using the Ansys CFD Fluent. The obtained results from the CFD study show that the recirculation flow (vortex) that appears in the aneurysm zone is affected by the size of the aneurysm [28]. Usmani and Patel conducted a numerical simulation of a healthy and a patient's cerebral artery with a saccular aneurysm. The simulation is done under exercise and rest states. The results show that the interaction of recirculated flow with the wall of the aneurysm presents abnormal distribution

for the WSS and the wall pressure. The patient under an exercise state has a high blood flow velocity which leads to an increase in the recirculation flow, wall pressure, and the WSS within the aneurysm [29]. Islami et al. performed a CFD study of the blood flow inside a simplified model of treated cerebral aneurysms with flow diverter stents (FDS). The numerical simulations were done on a simplified models of the carotid artery (one with FDS and one without). The simulations are conducted at $Re = 500$, with specific mass 1050 kg.m^{-3} . The blood described as incompressible Newtonian fluid with viscosity model (Carreau model). The results show enhancement for the flow patterns in the case with the FDS, which lead to expedite occlusion of the cerebral aneurysm. Enhancement the flow patterns lead to reduce the flow recirculation, wall pressure, and the WSS [30]. Souza et al. conducted a numerical study on an intracranial aneurysms model to investigate the blood flow and structure beside other parameters such as the wall's mechanical behavior. These parameters have the main influence on the aneurysm's rupture. The CFD simulations were done for the same model with four different Re values (1, 100, 500, and 1000). The problem is implemented using the commercial software Fluent, Ansys 2020 R2. The results of the investigations show that the flow recirculation at the aneurysms appears with increasing the Re value. Furthermore, the WSS, displacement, and strain have a maximum value at the highest Re [31].

In this paper, numerical simulations were performed for the intracranial aneurysms (IA) at anterior communicating artery. The remainder of the paper is organized as follows: In Sect. 2, the problem description, and the system of incompressible Navier–Stokes equations with a fully implicit finite element discretization are presented. Furthermore, the validation with the literature review is presented. The CFD studies were done using the commercial package Ansys Fluent 19.2 to investigate the blood flow parameters such as the WSS, wall pressure, and flow recirculation in Sect. 3. Moreover, the simulation is conducted on a simplified geometry (benchmark) of the IA, then the simulations upgraded to consider an actual brain aneurysm at the anterior communicating artery reconstructed from the MRI. Some concluding remarks are given in Sect. 4.

2 Numerical methods

2.1 Problem description

The CFD simulations in this work are consist of two different segments complement each other, as shown in the Fig. 1. The segment one is an investigation for the flow

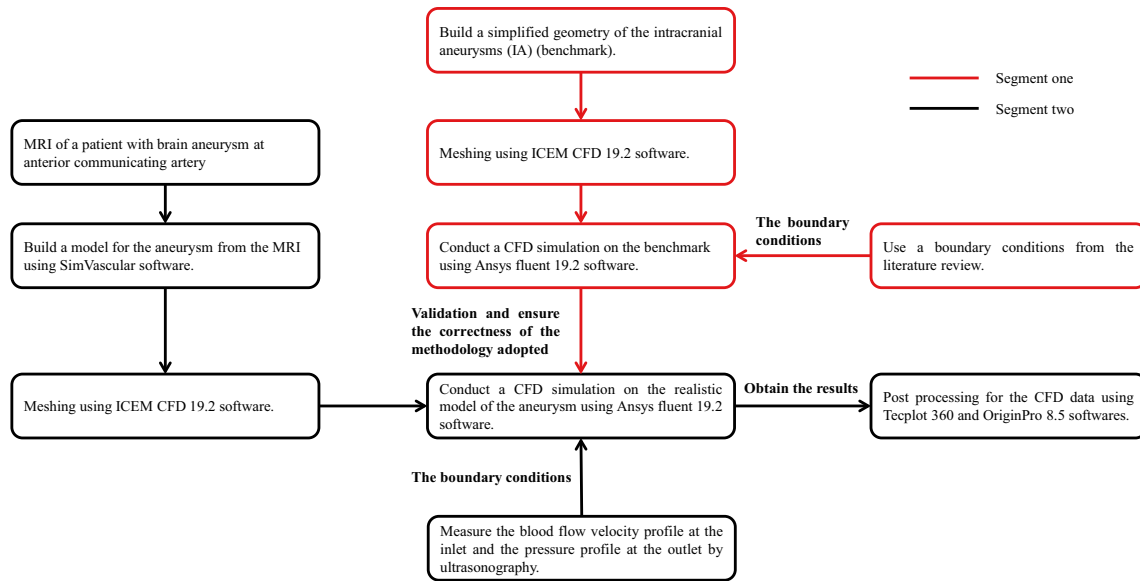


Fig. 1 Flow chart for CFD simulations of the blood flow in the brain aneurysm at anterior communicating artery

parameters of a simplified model of the IA (benchmark). The model is reconstructed and studied at boundary conditions based on the data from the literature [31]. In the segment two, an evaluation for the same parameters for a realistic model of an actual brain aneurysm at anterior communicating artery. The model reconstructed from the

MRI using SimVascular software. The boundary conditions used for the simulation such as the velocity profile at the inlet and the pressure profile at the outlet are obtained by ultrasonography. The computational studies for both segments are conducted to present the blood hemodynamics with similar CFD model adjustments, with changing the

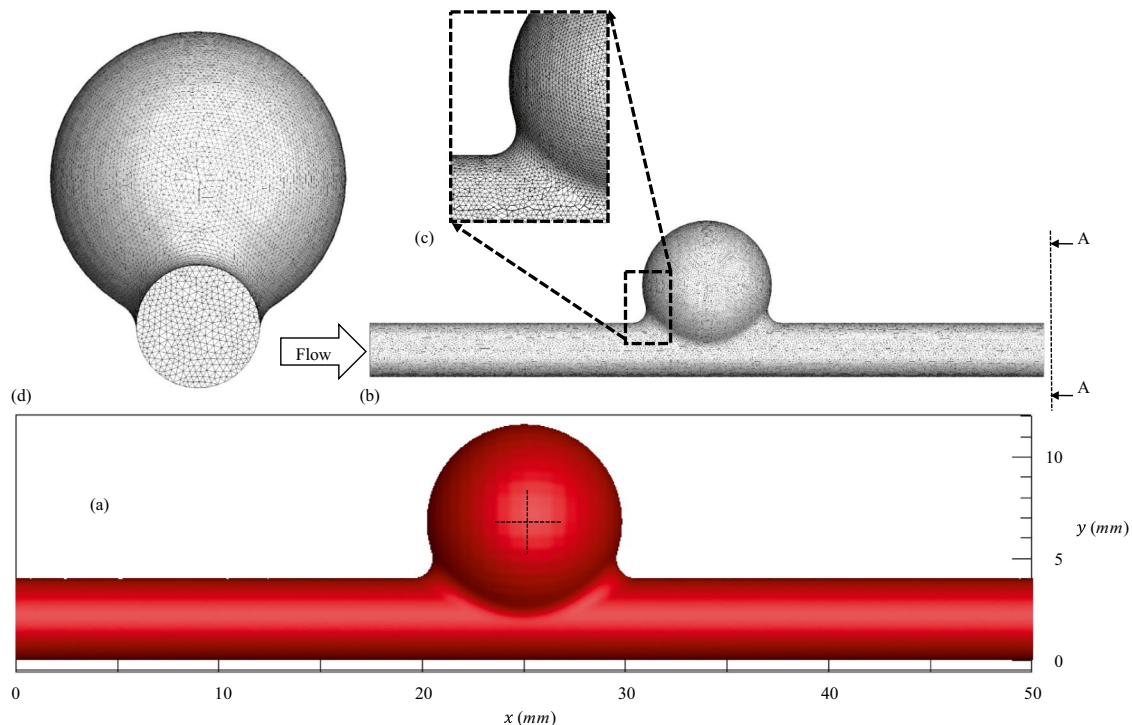


Fig. 2 a Schematic of the computational domain (the intracranial aneurysms (IA) benchmark model), b The computational mesh of the considered model, c Zoomed in view of the intracranial aneurysms mesh, and (D) Section A-A, Side view

velocity inlet, pressure outlet profile, and the geometry of the computational domain.

2.2 Governing equations and physical model

Steady-state three-dimensional CFD computations were performed for the considered geometry shown in Figs. 2a, 8. Differential equations governing the blood flow are given as in [32, 33]. The blood motion was governed by Navier–Stokes equations in the laminar flow condition as:

$$\Delta(\rho u) = 0 \tag{1}$$

$$\Delta(\rho uu) = -\frac{\partial p}{\partial x} + \Delta(\mu \nabla u) \tag{2}$$

$$\Delta(\rho uv) = -\frac{\partial p}{\partial y} + \Delta(\mu \nabla v) \tag{3}$$

$$\Delta(\rho uw) = -\frac{\partial p}{\partial z} + \Delta(\mu \nabla w) \tag{4}$$

where u, v, w are the blood flow velocities in x, y, z coordinates, respectively. The blood flow ρ is the blood specific mass while pressure defined as P . It is assumed that blood can be described as incompressible non-Newtonian fluid with viscosity model (Carreau model) and specific mass ρ of 1063 kg/m^3 . The wall of the blood vessels supposed to be rigid with no slipping ratio as shown in Tables 1 and 2 for the blood properties and Carreau model [31, 34]. It is noted that the Carreau fluid model treats the Newtonian fluid (blood flow in the present case). This means, at low shear rate the Carreau fluid model behaves as a Newtonian fluid model and at high shear rate behaves as a power law fluid. So, it is recommended for the blood artery simulation for accurate prediction [35]. It is noted that shear-thinning and wall shear stress with resistive impedance and their growth are successfully captured by using the Carreau fluid model. These assumptions account for the rigid wall model prescribed in the present simulation. The Carreau flow model equations can be found as follows [33].

Table 1 Blood flow properties used for the intracranial aneurysms (IA) benchmark model

Properties	Value (Unit)
Specific mass	1063 (Kg.m ⁻³)
Entrance velocity	888 (mm/s)
Outlet pressure (Gauge)	0 (Pa Gauge)

Table 2 Numerical values for the Carreau model

μ_∞ (Pa.s)	μ_0	n	λ (s)
1.0	0.436	0.36	3.3

$$\mu = H(t)(\mu_\infty + (\mu_0 - \mu_\infty)[1 + \gamma^2 \lambda^2]^{\frac{n-1}{2}}) \tag{5}$$

where $H(t)$ is the temperature dependence, known as the Arrhenius law.

$$H(t) = \exp\left[\alpha\left(\frac{1}{T - T_0}\right) - \left(\frac{1}{T_\alpha - T_0}\right)\right] \tag{6}$$

where α is the ratio of the activation energy to the thermodynamic constant and T_α is a reference temperature for which $H(t) = 1$. The T_0 is the temperature shift, is set to 0 by default, and corresponds to the lowest temperature that is thermodynamically acceptable. The λ is the time constant.

In the current work, the simulations done in the two segments using the commercial package Ansys Fluent 19.2 software [33] to solve the governing differential equations in the three-dimensional computational domain. The Re used is less than 2300, which means that the flow is laminar. Second-order upwind schemes are used for all conservation equations. The pressure–velocity coupling used a coupled scheme, and the pressure is calculated with the second-order scheme. That coupling scheme solves the momentum and pressure-based continuity equations together. The pseudo transient for fluid and solid zones are 0.7 and 1.0, respectively. The pseudo transient scheme is used to accomplish strong convergence which is favorable for the complicated flow of the blood.

2.3 Mesh

A grid independence study is performed to ensure the computational results and the generated mesh is shown in Figs. 2b, c, d, and 8e. For the segment one, 522,323 tetrahedral mesh used for grinding the IA benchmark. For the segment two, 722,724 tetrahedral mesh used for grinding the realistic aneurysm model. The size and number of elements used obtained from CFD study at the literature [10]. For all meshes at the segment one and two, the mesh was refined and y^+ is approximate 1.

Table 3 The pressure drop across the intracranial aneurysms benchmark model, in comparison of the published results

Reference	$P_{in} - P_{out}$
Souza et al. (2022) [31]	726.120 (Pa)
Present	749.802 (Pa)
Error (%)	3.15

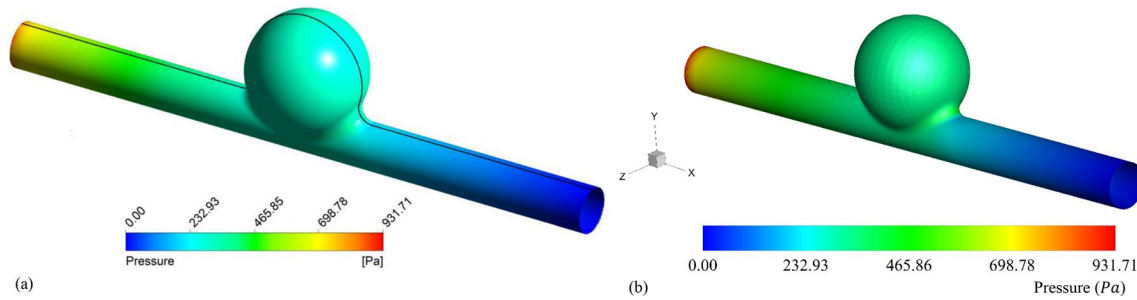


Fig. 3 The distribution wall pressure for the intracranial aneurysms (IA) benchmark model at inlet velocity flowrate=888 mm/s, for **a** the published results in [31], and **b** present work

2.4 Validation

The results obtained from the CFD simulation validated the literature results [31]. In Table 3, the pressure drop across the IA benchmark model in the present work shows a 3.261% error by comparing it with the literature [31]. Moreover, Fig. 3 shows visual aid for the validation of the results, which report the wall pressure contours of the present and the literature studies. This validation grantee that the present CFD simulations are capable to evaluate the hemodynamics, especially for the aneurysm. The relative error between the obtained pressure difference and that of the literature Souza et al. [31], is given by $\frac{|749.802-726.120|}{726.120} * 100 = 3.15\%$.

3 Results and discussions

3.1 Segment one, Results for the simplified IA (benchmark) model

In this part, a comprehensive investigation for the blood flow parameters such as the wall pressure, recirculation flow, and the WSS within IA model are presented.

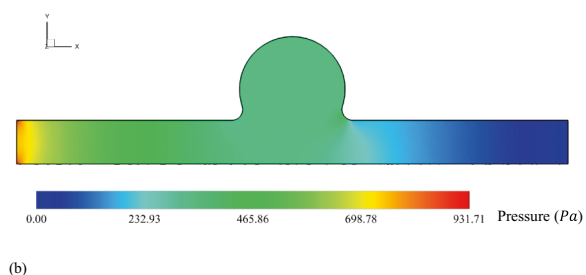
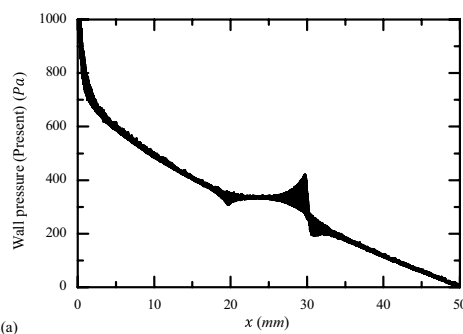


Fig. 4 Wall pressure magnitude profile **a** along x axis and **b** xy section of pressure contour

3.1.1 The pressure distribution

In Figs. 3 and 4, the value of the wall pressure decreased in the direction of the blood flow except for the aneurysms zone. The value of the wall pressure at the beginning of that zone remain constant due to the present of the recirculation flow inside the aneurysms. The flow starts to reverse at the rear edge region of the aneurysms as result of the flow-wall interaction at that zone. The interaction with the edge and the surrounding wall lead to increase the wall pressure value.

3.1.2 The flow structures

The blood flow velocity have a significant impact on the presence of the recirculation flow, which by increasing the velocity the presence of flow recirculation will be noted [29, 31]. In Fig. 5, two types of flow regimes appeared. The laminar flow regime appeared close to the inlet and the outlet of the vessel, and the recirculation flow (vortex formation) appeared close and inside the bulge. The recirculation flow in the aneurysms zone presented due to using high flow velocity (888 mm/s). The flow recirculation presented due to separation at the aneurysms rear edge.

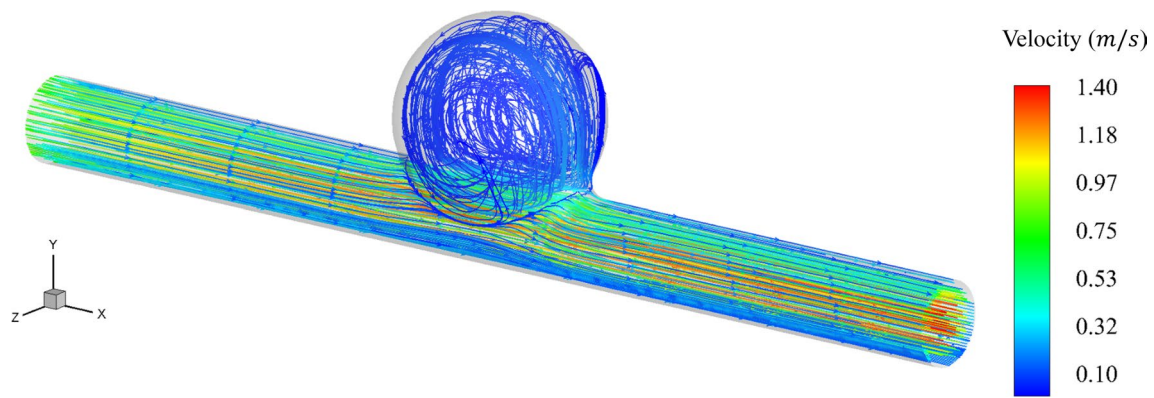


Fig. 5 3D velocity streamlines for the intracranial aneurysms (IA) benchmark model, which show the recirculation of the flow at aneurysms

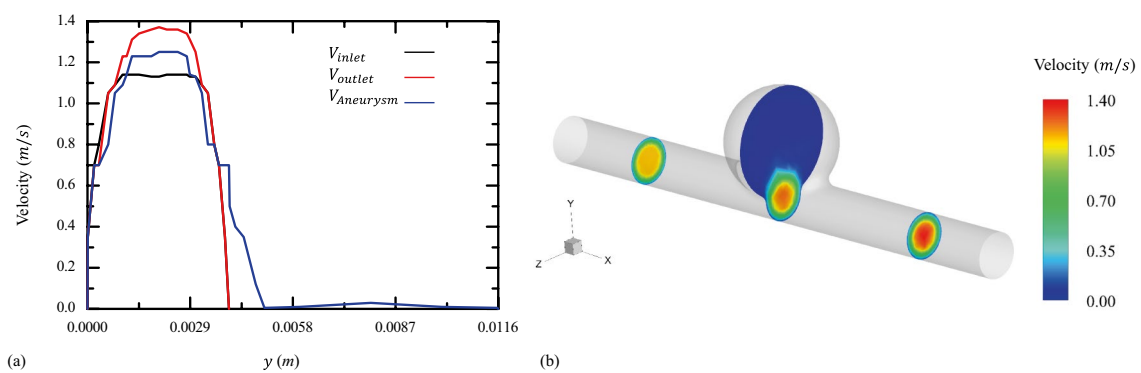


Fig. 6 **a** Absolute velocity profiles at three different regions for the intracranial aneurysms (IA) benchmark model **b** Three cutting planes corresponding to the curves in **(a)**, respectively

In Fig. 6, three absolute velocity profiles with y axis at three cutting. The three cutting in the x direction show the velocity magnitude contour at different positions (inlet, outlet, and the aneurysms). The velocity profile at the inlet and the outlet shows a symmetric distribution around the center of the cylinder y axis. The flow profile at the inlet has a developing velocity profile, and that ensure the methodology adopted, which the flow inlet have a plug velocity boundary condition. The velocity profile at the outlet has a fully developed velocity profile. The present of the saccular aneurysm leads to change in the velocity profile symmetry. The right side of the aneurysm velocity profile shows that the velocity value decreased comparing to the velocity at the center of the cylinder. The absolute value of the velocity magnitude increased at the y axis range of (6 mm—9 mm), which indicate to the core of the vortex formation.

3.1.3 The wall shear stress (WSS)

The wall shear stress around the bulge was investigated in Fig. 7. The behavior of the WSS is qualitatively similar for the

wall pressure distribution shown in Figs. 3 and 4. The value of the WSS decreased in the flow direction except for the bulge zone. The value of the WSS at the beginning of the aneurysms zone remain constant due to the presence of the recirculation flow. The value of the WSS increases at the outlet of the bulge due to the flow interaction and separation at the rear edge.

3.2 Segment two, results for the realistic model of an actual brain aneurysm at anterior communicating artery

In this part, a CFD simulation are done on a realistic model of an actual brain aneurysm at anterior communicating artery reconstructed from the MRI of patient specific artery as shown in Fig. 8. The computational domain reconstructed using the SimVascular software as discussed in the methodology. The size of the aneurysm is 9.91 mm, 6.62 mm, and 8.082 mm in yz , xy , and xz planes, respectively. The change of the cross section from the main vessel branch to the aneurysm have a significant increasing

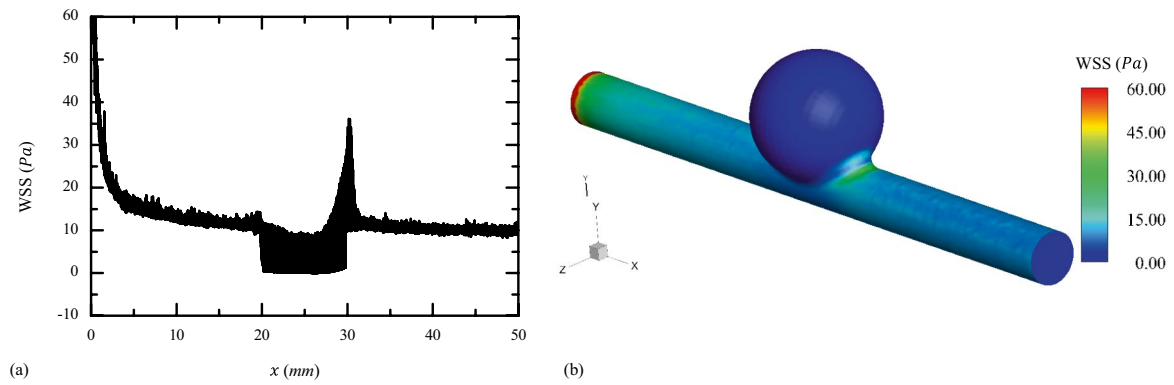


Fig. 7 **a** Wall shear stress (WSS) magnitude profile **b** Wall shear stress (WSS) magnitude distribution along the intracranial aneurysms (IA) benchmark model, respectively

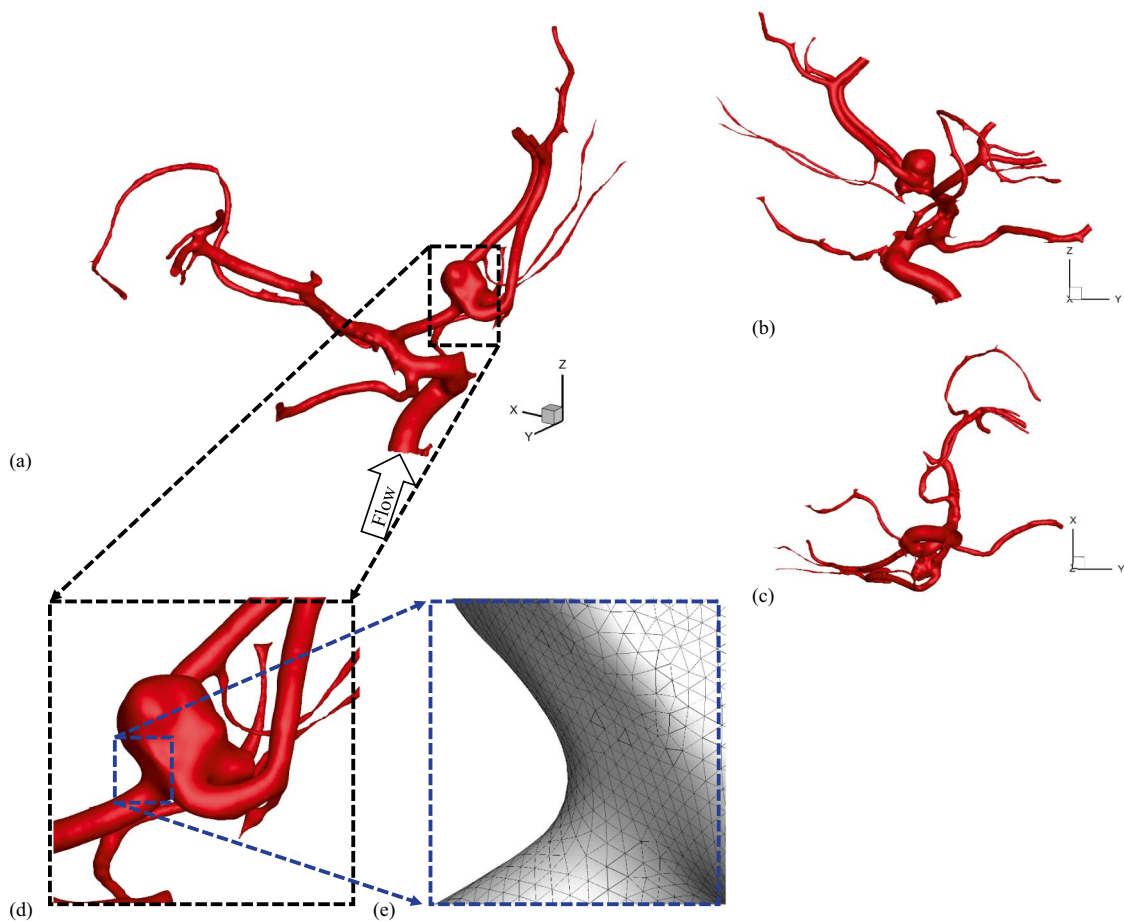


Fig. 8 **a** The computational domain, **b**, **c** side view of the computational domain at yz , xy planes, respectively, **d** Zoomed in view for the brain aneurysm at anterior communicating artery, and **e** a magnified view of the computational mesh

which approximately 200% in the yz plane, as shown in Fig. 9.

Furthermore, at segment two the inlet velocity and the outlet pressure profiles are different than the ones

used at the segment one. The boundary conditions of the simulation based on measured values of the blood flow velocity profile at the inlet and the pressure profile at the outlet by ultrasonography as shown in Figs. 10 and

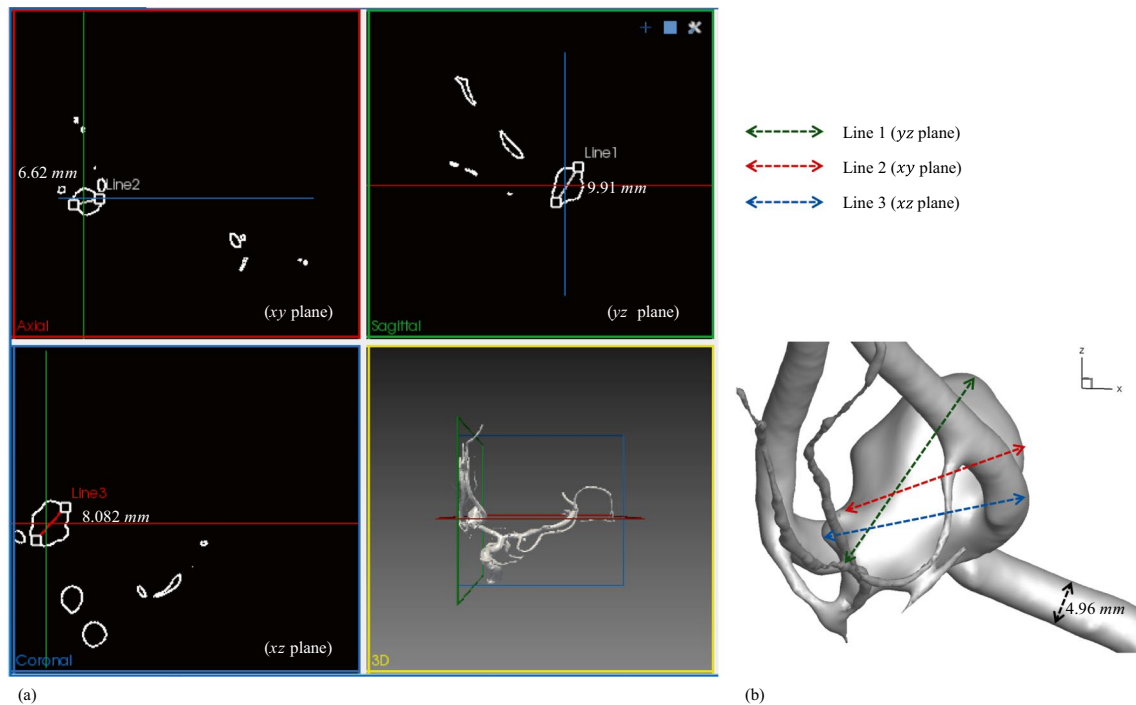


Fig. 9 **a** The size of the aneurysm in the planes (yz, xy, and xz), 3D geometry, and **b** the size of the inlet vessel

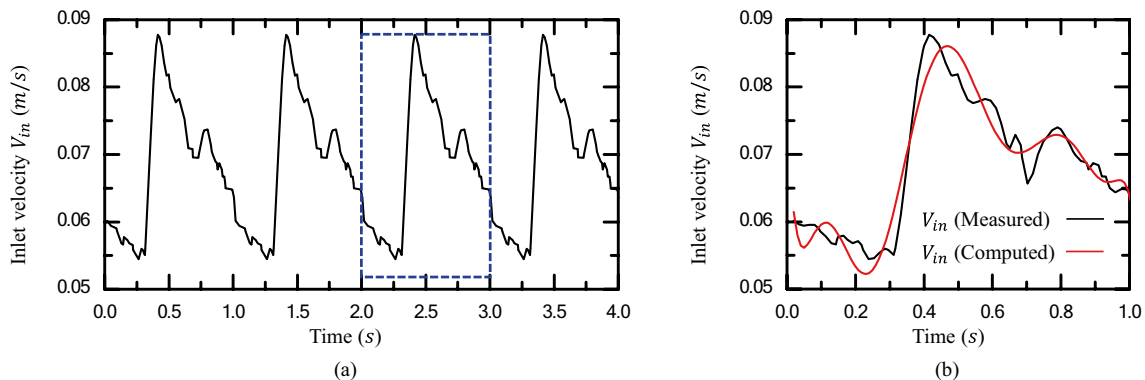


Fig. 10 The velocity profiles imposed on the anterior communicating artery inlets

11. The blood flow parameters investigated in that part is the same ones discussed in the segment one.

3.2.1 The flow structure

The aneurysm at anterior communicating artery led to present the recirculation flow (vortex formation) which affects a lot on the WSS, wall pressure, and outlet flow regimes. In Fig. 12, away from the aneurysm, the flow at the inlet and the outlet of the main artery have a laminar flow, which is presented in Fig. 5 at the segment one. The flow interaction with the wall of the bulge leads

to present the flow separation. At the separation region, the value of the wall pressure and the WSS achieve the highest values in that zone.

In Fig. 13, two cuts in the bulge show the velocity magnitude contour at the aneurysm zone at yz and xz planes, respectively. At the yz plane, the maximum velocity appears at the inlet and decreases gradually in the z direction, except for the zone of the vortex formation. In Fig. 13c, the velocity distribution vector shows the interaction of the flow with the bulge wall, which leads to reverse flow responsible for the vortex formation at the z direction. At the xz plane, the maximum value of the velocity magnitude

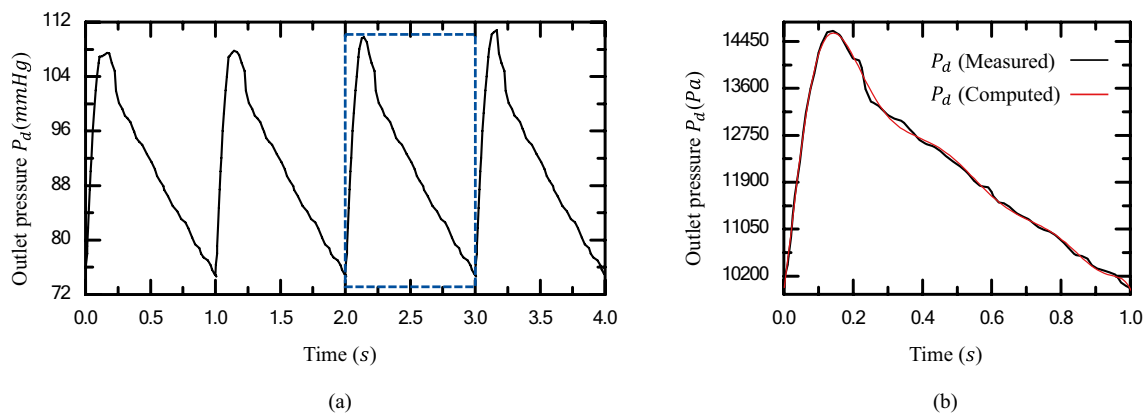


Fig. 11 The pressure profiles imposed on the anterior communicating artery outlets in **a** mmHg and **b** Pa

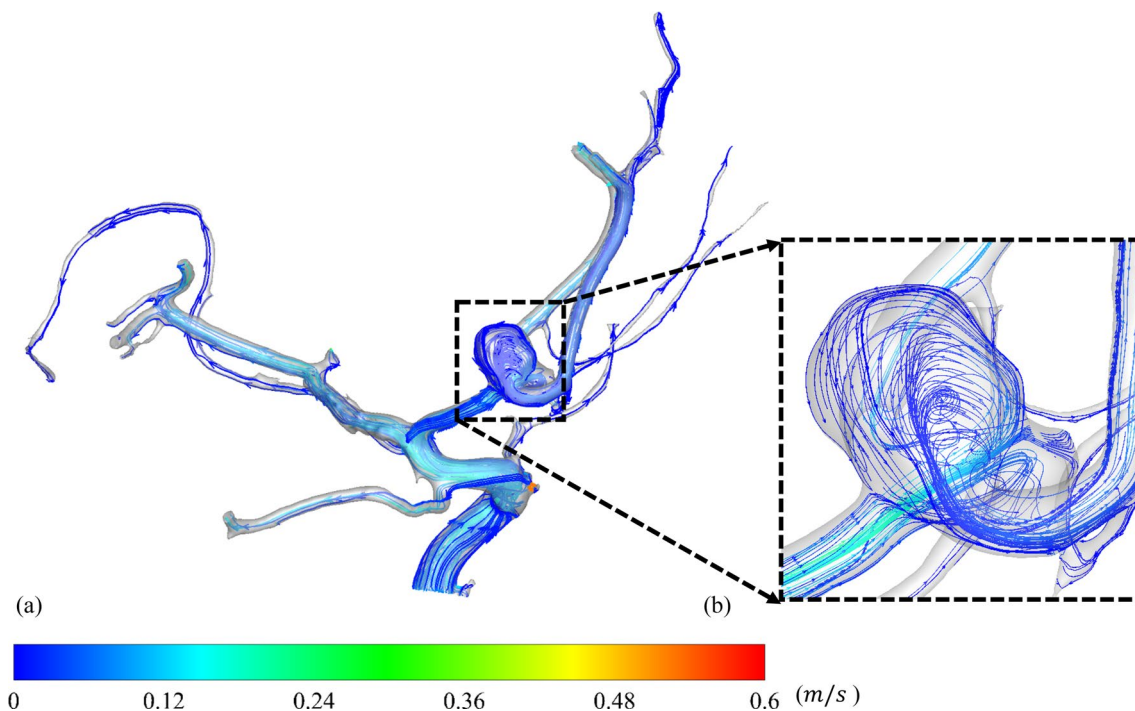


Fig. 12 **a** The velocity streamlines for the anterior communicating artery **b** Zoomed in view for the aneurysm

at the core of the flow inlet and decrease gradually in the z direction except for the value next to the wall in the x direction. The value of the velocity is high next to the wall in the right part of the x direction compared to the velocity in the same level of x direction due to the present of the recirculation flow next to the flow-wall interaction zone, as shown in Figs. 13b and d.

3.2.2 Hemodynamics wall parameters

The investigation of the wall parameters such as the WSS and the wall pressure have a significant value to

understand the aneurysm rupture. In Figs. 14 and 15, the values of wall parameters affected by the blood flow regimes. The value of the WSS and the wall pressure decreased gradually in the blood flow pass except for the aneurysm zone, which presented in the simplified model at segment one (Figs. 4 and 7). In Figs. 14b and c, the WSS is much higher near the bulge zone inlet comparing to the outlet zone. The WSS increases at the outlet edges due to the flow interaction with the edges. The variation of WSS help to expect the location of the aneurysm ruptured. The investigations state that the rupture would occurs at low wall shear stress region [36].

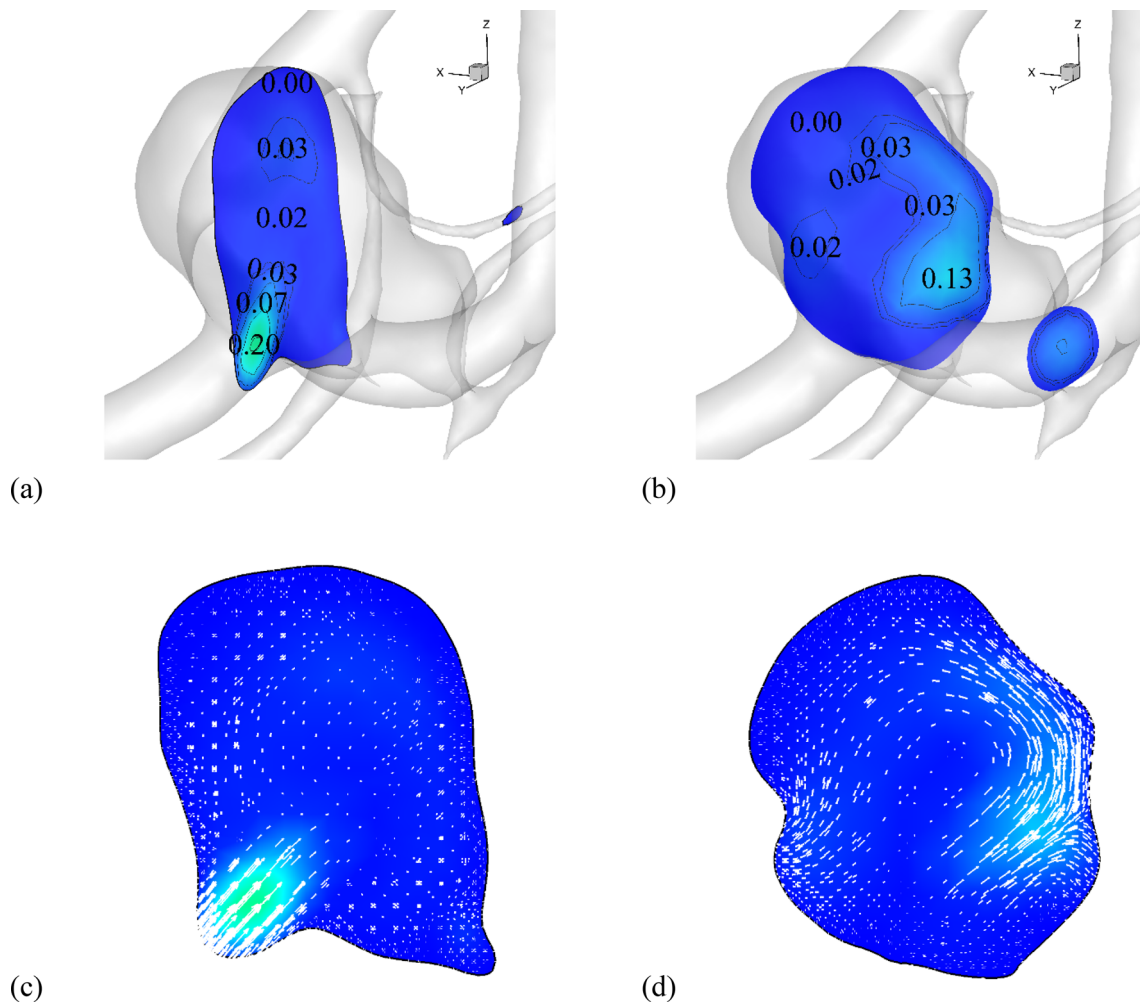


Fig. 13 Contours of the velocity distribution at **a** yz-plane and **b** xz-plane. Cross section views of velocity distribution vector at **c** yz plane and **d** xz plane, respectively

Furthermore, the change in the cross-section of the blood vessel has a significant impact on the WSS. The aneurysm is not only blood vessel disease that appears due to the change in the cross-section area. The presence of stenosis influences the WSS values, where the presence of the stenosis increases the value of the WSS at the stenosis zone, Fig. 14d. After the contraction zone, the WSS values were reduced with increasing the cross-section area of the blood vessel [34, 37].

4 Conclusion

In this paper, the CFD simulations are conducted to investigate the hemodynamics of the flow for a patient with a brain aneurysm at anterior communicating artery using

two geometrical models (ideal and realistic geometry) and Newtonian model with viscosity model (Carreau model). The approach of using a simplified (benchmark) geometry of the aneurysm helped to understand the hemodynamics inside the complex geometry of the realistic model. It is observed that, the presence of the aneurysms in the patient's vascular system lead to recirculation flow inside the bulge. The flow-wall interaction due to the flow recirculation produce uneven variation in the wall shear stress, which help to investigate the region of the rupture. The obtained results investigate that the wall pressure and the WSS achieve the highest values at the flow-wall interaction zone. The wall pressure and the WSS behaviors are qualitatively similar. The presence of stenosis increases the WSS at the contraction zone.

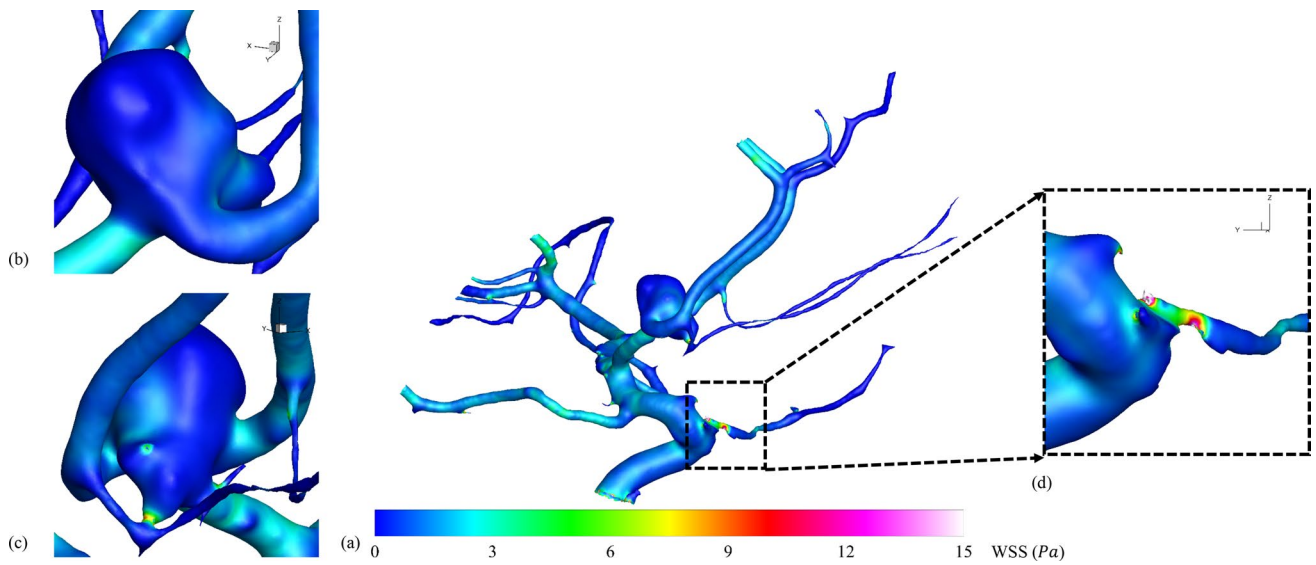
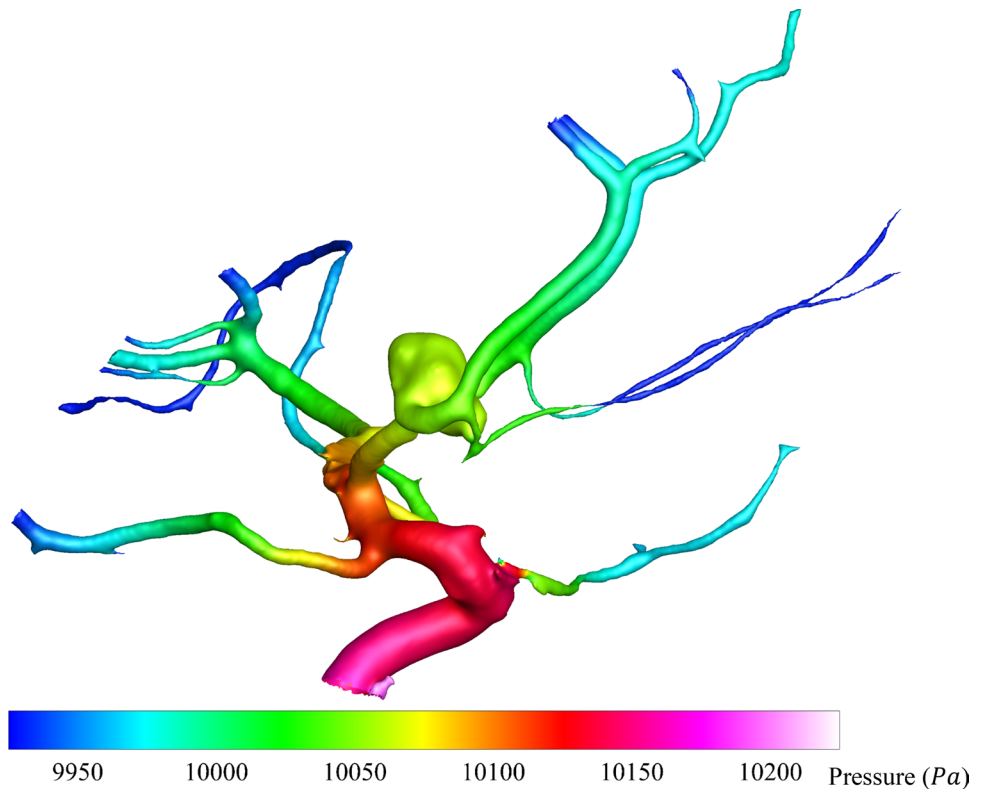


Fig. 14 **a** The wall shear stress distribution along the patient’s blood vessels. zoom in view of **(b)** the area near the aneurysm inlet, **c** the area near the aneurysm outlet, and **d** the area near the stenosis

Fig. 15 The pressure distribution along the patient’s blood vessels



Acknowledgements This work was partially supported by the Science and Technology Development Fund (STDF) of Egypt, project No: 39385.

Authors’ contributions AGR: Conceptualization, methodology, data curation, model building, simulation, validation, visualization, figure preparation, draft preparation, and draft revision. TA:

Conceptualization, methodology, draft revision, commenting, Supervision.

Funding Open access funding provided by The Science, Technology & Innovation Funding Authority (STDF) in cooperation with The Egyptian Knowledge Bank (EKB).

Data availability The data that support the findings of this study are available from the corresponding author upon reasonable request.

Declarations

Conflict of interest The authors declare that they have no conflict of interest.

Open Access This article is licensed under a Creative Commons Attribution 4.0 International License, which permits use, sharing, adaptation, distribution and reproduction in any medium or format, as long as you give appropriate credit to the original author(s) and the source, provide a link to the Creative Commons licence, and indicate if changes were made. The images or other third party material in this article are included in the article's Creative Commons licence, unless indicated otherwise in a credit line to the material. If material is not included in the article's Creative Commons licence and your intended use is not permitted by statutory regulation or exceeds the permitted use, you will need to obtain permission directly from the copyright holder. To view a copy of this licence, visit <http://creativecommons.org/licenses/by/4.0/>.

References

1. Nixon AM, Gunel M, Sumpio BE (2010) The critical role of hemodynamics in the development of cerebral vascular disease. *J Neurosurg* 112:1240–1253. <https://doi.org/10.3171/2009.10.jns09759>
2. Cecchi E, Giglioli C, Valente S, Lazzeri C, Gensini GF, Abbate R et al (2011) Role of hemodynamic shear stress in cardiovascular disease. *Atherosclerosis Elsevier Ireland Ltd* 214:249–256. <https://doi.org/10.1016/j.atherosclerosis.2010.09.008>
3. Rahma AG, Yousef K, Abdelhamid T (2022) Blood flow CFD simulation on a cerebral artery of a stroke patient. *SN Appl Sci* 4:261. <https://doi.org/10.1007/s42452-022-05149-y>
4. Xiang J, Natarajan SK, Tremmel M, Ma D, Mocco J, Hopkins LN et al (2011) Hemodynamic-morphologic discriminants for intracranial aneurysm rupture. *Stroke* 42:144–152. <https://doi.org/10.1161/strokeaha.110.592923>
5. Elhanafy A, Guaily A, Elsaid A (2019) Numerical simulation of Oldroyd-B fluid with application to hemodynamics. *Adv Mech Eng* 11:1–7. <https://doi.org/10.1177/1687814019852844>
6. Karmonik C, Yen C, Grossman RG, Klucznik R, Benndorf G (2009) Intra-aneurysmal flow patterns and wall shear stresses calculated with computational flow dynamics in an anterior communicating artery aneurysm depend on knowledge of patient-specific inflow rates. *Acta Neurochir* 151:479–485. <https://doi.org/10.1007/s00701-009-0247-z>
7. Boutsianis E, Guala M, Olgac U, Wildermuth S, Hoyer K, Ventikos Y et al (2009) CFD and PTV steady flow investigation in an anatomically accurate abdominal aortic aneurysm. *J Biomech Eng* 131:1–15. <https://doi.org/10.1115/1.3002886>
8. Ford MD, Nikolov HN, Milner JS, Lownie SP, DeMont EM, Kalata W et al (2008) PIV-measured versus CFD-predicted flow dynamics in anatomically realistic cerebral aneurysm models. *J Biomech Eng* 130:1–9. <https://doi.org/10.1115/1.2900724>
9. Hoi Y, Woodward SH, Kim M, Taulbee DB, Meng H (2006) Validation of CFD simulations of cerebral aneurysms with implication of geometric variations. *J Biomech Eng* 128:844–851. <https://doi.org/10.1115/1.2354209>
10. Luo L, Shiu WS, Chen R, Cai XC (2019) A nonlinear elimination preconditioned inexact Newton method for blood flow problems in human artery with stenosis. *J Comput Phys*. <https://doi.org/10.1016/j.jcp.2019.108926>
11. Nordgaard H, Swillens A, Nordhaug D, Kirkeby-Garstad I, Van Loo D, Vitale N et al (2010) Impact of competitive flow on wall shear stress in coronary surgery: computational fluid dynamics of a LIMA-LAD model. *Cardiovasc Res Engl* 88:512–519. <https://doi.org/10.1093/cvr/cvq210>
12. Lin KY, Shih TC, Chou SH, Chen ZY, Hsu CH, Ho CY (2016) Computational fluid dynamics with application of different theoretical flow models for the evaluation of coronary artery stenosis on CT angiography: comparison with invasive fractional flow reserve. *Biomed Phy Eng Exp* 2:1–11. <https://doi.org/10.1088/2057-1976/2/6/065011>
13. Shanmugavelayudam SK, Rubenstein DA, Yin W (2010) Effect of geometrical assumptions on numerical modeling of coronary blood flow under normal and disease conditions. *J Biomech Eng* 132:61004. <https://doi.org/10.1115/1.4001033>
14. Katritsis D, Kaiktsis L, Chaniotis A, Pantos J, Efstathopoulos EP, Marmarelis V (2007) Wall shear stress: theoretical considerations and methods of measurement. *Prog Cardiovasc Dis* 49:307–329. <https://doi.org/10.1016/j.pcad.2006.11.001>
15. Murayama Y, Fujimura S, Suzuki T, Takao H (2019) Computational fluid dynamics as a risk assessment tool for aneurysm rupture. *Neurosurg Focus*. <https://doi.org/10.3171/2019.4.focus19189>
16. Morris PD, Narracott A, Von Tengg-Kobligh H, Soto DAS, Hsiao S, Lungu A et al (2016) Computational fluid dynamics modelling in cardiovascular medicine. *Heart* 102:18–28. <https://doi.org/10.1136/heartjnl-2015-308044>
17. Wellnhofer E, Osman J, Kertzsch U, Affeld K, Fleck E, Goubergrits L (2010) Flow simulation studies in coronary arteries—impact of side-branches. *Atheroscler Int* 213:475–481. <https://doi.org/10.1016/j.atherosclerosis.2010.09.007>
18. Cezbal JR, Mut F, Chung BJ, Spelle L, Moret J, Van Nijnatten F et al (2017) Understanding angiography-based aneurysm flow fields through comparison with computational fluid dynamics. *Am J Neuroradiol* 38:1180–1186
19. Xiang J, Tutino VM, Snyder KV, Meng H (2014) CFD: Computational fluid dynamics or confounding factor dissemination? the role of hemodynamics in intracranial aneurysm rupture risk assessment. *Am J Neuroradiol* 35:1849–1857. <https://doi.org/10.3174/ajnr.a3710>
20. Bauer A, Bopp M, Jakirlic S, Tropea C, Krafft AJ, Shokina N et al (2020) Analysis of the wall shear stress in a generic aneurysm under pulsating and transitional flow conditions. *Exp Fluids* 61:1–16. <https://doi.org/10.1007/s00348-020-2901-4>
21. Levitt MR, Barbour MC, Du Roscoat SR, Geindreau C, Chivukula VK, McGah PM, Nerva JD, Morton RP, Kim LJ, Aliseda A (2017) Computational fluid dynamics of cerebral aneurysm coiling using high-resolution and high-energy synchrotron X-ray microtomography: Comparison with the homogeneous porous medium approach. *J NeuroIntervent Surg* 9:777–782. <https://doi.org/10.1136/neurintsurg-2016-012479>
22. Iimuro Y, Suzumura K, Ohashi K, Tanaka H, Iijima H, Nishiguchi S et al (2015) Hemodynamic analysis and treatment of an enlarging extrahepatic portal aneurysm: report of a case. *Surg Today* 45:383–389. <https://doi.org/10.1007/s00595-014-0882-8>
23. Thompson BG, Brown RD, Amin-hanjani S, Broderick JP, Cockroft KM, Connolly ES, et al (2015) AHA / ASA Guideline guidelines for the management of patients with unruptured intracranial aneurysms. <https://doi.org/10.1161/str.0000000000000070>
24. Schievink WI (1997) Intracranial aneurysms. *The New Engl Med* 336:28–40. <https://doi.org/10.1056/nejm199701023360106>
25. Johnston SC, Higashida RT, Barrow DL, Caplan LR, Dion JE, Hademenos G, et al. (2002) Recommendations for the endovascular treatment of intracranial aneurysms a statement for healthcare

- professionals from the committee on. pp. 2536–44. <https://doi.org/10.1161/01.str.0000034708.66191.7d>
26. Amenta PS, Yadla S, Campbell PG, Maltenfort MG, Dey S, Ghosh S et al (2012) Analysis of nonmodifiable risk factors for intracranial aneurysm rupture in a large, retrospective cohort. *Neurosurgery* 70:693–701. <https://doi.org/10.1227/neu.0b013e3182354d68>
 27. MacDonald DE, Najafi M, Temor L, Steinman DA (2022) Spectral Bandedness in high-fidelity computational fluid dynamics predicts rupture Status in intracranial aneurysms. *J Biomech Eng* 10(1115/1):4053403
 28. Shishir SS, Miah MAK, Islam AKMS, Hasan ABMT (2015) Blood flow dynamics in cerebral aneurysm - A CFD simulation. *Procedia Engineering* 105:919–927. <https://doi.org/10.1016/j.proeng.2015.05.116>
 29. Usmani AY, Patel S (2018) Hemodynamics of a cerebral aneurysm under rest and exercise conditions. *Int J Energy for a Clean Environ* 19:119–136. <https://doi.org/10.1615/InterJEnerCleanEnv.2018020888>
 30. Baheri Islami S, Wesolowski M, Revell W, Chen X (2021) Virtual reality visualization of CFD simulated blood flow in cerebral aneurysms treated with flow diverter stents. *Appl Sci*. <https://doi.org/10.3390/app11178082>
 31. Souza MS, Souza A, Carvalho V, Teixeira S, Fernandes CS, Lima R et al (2022) Fluid flow and structural numerical analysis of a cerebral aneurysm model. *Fluids*. <https://doi.org/10.3390/fluid57030100>
 32. Versteeg HK (1955) *An Introduction to Computational Fluid Dynamics: the Finite Volume Method*. Harlow, Essex, England; Longman sci technol: New York: Wiley
 33. Fluent A (2013) *Ansys fluent theory guide*. ANSYS Inc, USA 15317:724–746
 34. Zouggari L (2018) The role of biomechanics in the assessment of carotid atherosclerosis severity: a numerical approach OPEN ACCESS. *World J Vascular Surg* 1:1007
 35. Akbar NS, Nadeem S (2014) Carreau fluid model for blood flow through a tapered artery with a stenosis. *Ain Shams Eng J* 5:1307–1316
 36. Yoshiki K, Misaki K, Nambu I, Fukui I, Mohri M, Uchiyama N et al (2017) Intraoperative rupture of unruptured cerebral aneurysm during craniotomy: a case report. *Case Rep Neurol* 9:261–266. <https://doi.org/10.1159/000480425>
 37. Xie X, Li Y, Xie S (2018) Computation of hemodynamics in eccentric coronary stenosis: a morphological parametric study. *Technol Health Care* 26:229–238. <https://doi.org/10.3233/thc-160529>

Publisher's Note Springer Nature remains neutral with regard to jurisdictional claims in published maps and institutional affiliations.